Fatigue Evaluation of Carbon FRP-Reinforced Porous Asphalt Composite System Using a Model Mobile Load Simulator

Hyunwook Kim *
Scientist (*Corresponding Author)
Laboratory for Road Engineering and Sealing Components
Empa, Swiss Federal Laboratories for Materials Testing and Research,
Überlandstrasse 129, CH-8600, Dübendorf, Switzerland
Phone: +41-44-823-4474
Fax: +41-44-821-6244
email: hyunwook.kim@empa.ch

Kirill Sokolov
Research Engineer
Laboratory for Road Engineering and Sealing Components
Empa, Swiss Federal Laboratories for Materials Testing and Research,
Überlandstrasse 129, CH-8600, Dübendorf, Switzerland
email: kirill.sokolov@empa.ch

Lily D. Poulikakos
Research Engineer
Laboratory for Road Engineering and Sealing Components
Empa, Swiss Federal Laboratories for Materials Testing and Research,
Überlandstrasse 129, CH-8600, Dübendorf, Switzerland
email: lily.poulikakos@empa.ch

Manfred N. Partl
Head of Laboratory
Laboratory for Road Engineering and Sealing Components
Empa, Swiss Federal Laboratories for Materials Testing and Research,
Überlandstrasse 129, CH-8600, Dübendorf, Switzerland
email: manfred.partl@empa.ch

Date of Resubmission: February 16, 2009

Submitted for Presentation at the TRB 88th Annual Meeting and Publication in the Transportation Research Record 2009: Journal of the Transportation Research Board

Number of words: 3619 + 3750 (11 figures + 4 tables) = 7369

* Final version

ABSTRACT

Porous asphalt (PA) has been widely used in many countries because of its positive benefits such as efficient water drainage, improved safety in wet weather conditions, and noise reduction. However, the attractive features of PA do not last for a long time due to the performance degrading of PA caused by clogging, stripping, and accelerated aging. Application of fiber reinforcement materials can be a possible solution to overcome the structural weakness in porous asphalt pavements. This paper focuses on the fatigue investigation of fiber-reinforced porous asphalt composite systems using a model mobile load simulator (MMLS). Carbon fiber reinforcement polymer (FRP) grids were used to strengthen the fatigue resistance of porous asphalt. To this end, FRP were placed between two asphalt layers as a reinforcement interlayer. The dynamic fatigue traffic loadings were applied on the top surface of reinforced specimens to investigate the performance improvement by reinforcement materials. These fatigue tests were conducted under four different conditions: unreinforced and reinforced at dry; unreinforced and reinforced at wet. During the fatigue tests, transverse and longitudinal strains at the bottom of specimen were measured by installed strain gauges and the transverse profiles of surface deflection were periodically measured in the middle of specimen by the profilometer. The coaxial shear test (CAST) was conducted to characterize the complex modulus of porous asphalt and the stiffness changes by aging and water conditioning. The stiffness difference between unaged and aged specimens was 25% at minimum and 55% at maximum. The surface deflection of porous asphalt was successfully reduced by 23% at dry and by 48% at wet conditions using interlaid carbon FRP grids. In addition, the reinforcement layer could increase the fatigue life by 23% at dry and by 27% at wet conditions based on MMLS test results.

Keyword: Porous asphalt, Fatigue, Composite, Carbon FRP grids, MMLS, CAST

INTRODUCTION

Porous asphalt (PA) or open graded friction course (OGFC) asphalt has widely been used for water drainage and noise reduction in order to improve traffic safety and comfort for both drivers and residents living in the vicinity of roads. PA consists mainly of coarse aggregates with small amounts of sand and filler, thus creating an open texture and a permeable structure with high porosity. Due to its rough surface texture and large amount of pores in its mixture, porous asphalt improves skid resistance and provides good visibility while reducing spray and splash on wet surfaces. The traffic noise level on the roads is also reduced considerably. Porous asphalt in Europe typically has air void contents in the order of 20%. Switzerland also started using porous asphalt (called drainasphalt DRA in German or asphalt drainant in French) from 1979 along Swiss motorways. Based on the survey taken in 2004, eight of 26 Cantons in Switzerland used PA on the roads and a third of Canton Vaud motorways were covered with porous asphalt (1-3).

Despite its environmental benefits, porous asphalt can suffer from several factors, which can affect both its performance and its service life (4-6). One of the most critical factors is the continuous exposure of binder film on the aggregate surface to oxygen, sunlight, and water. This can result in binder hardening by aging and the reduction of pavement service life by moisture damage (7). When asphalt hardens, aggregates can be stripped easily from asphalt mixtures. It is well known that, due to its high porosity, PA can age much faster than conventional dense mixtures. Results of full-scale road trials in England demonstrate that the life of porous asphalt is ultimately limited by binder hardening with material failures when its penetration index drops below 15 (8). Another critical factor is the water infiltration into the air void and binder film of PA mixture. Rain water penetrates through the porous matrix and it sometimes remains in the pavement layer keeping the asphalt in wet conditions for a long time. This moisture can cause some extra damage in porous asphalt by stripping the binder film from the aggregate surfaces. The structural capability of PA under heavy traffic loadings is debatable. The investigation by Potter and Halliday (9) showed that 40mm thickness of porous wearing course was equivalent to the structural capability of 20mm hot rolled asphalt (HRA). Also, the Swiss standard suggests that 10mm thickness of the traditional Swiss base course mixture (HMT) is equal to 15mm of PA, and that the structural contribution of PA is equal to 65% strength of other surface mixtures, including mastic asphalt and stone mastic asphalt (SMA) (10). Dutch and Belgian researches concluded that, in comparison to dense mixtures, the layer thickness equivalent factor of 0.8 to 1.0 can be assigned to PA (11). In Japan, PA is assigned with the same equivalency factor as for other asphalt layers because there is no significant difference in terms of durability from their own trial pavement sections (12).

The objective of this study is to investigate the fatigue behavior of fiber-reinforced porous asphalt composites using a model mobile load simulator (MMLS). Carbon fiber reinforcement polymer (FRP) grids were used as a reinforcement interlayer to increase the structural capability and the fatigue resistance. The reinforced and unreinforced porous asphalt composite systems were compared at both dry and wet conditions to characterize the performance improvement by carbon FRP grids and to investigate the water sensitivity of reinforced porous asphalt composites. Also, the complex modulus of PA was obtained from the coaxial shear test (CAST), developed by Swiss federal laboratories for materials testing and research (Empa).

MATERIALS

The Swiss standard, SN 640431-7a, contains requirements for surface course, base course, and drainage courses. It lists volumetric requirements such as mineral gradation, air void contents, and water permeability. In 2005, Switzerland had adopted the European specifications for PA (13). The Swiss standards for PA recommended an 11 mm nominal maximum aggregate size (NMAS) with thickness of 30mm to 50mm for the surface layer. For the surface layer of high volume roads, only polymer modified binder should be used in PA. The requirement of air void content is 22% for surface layer and 15% for base layer. The most common PA in Switzerland, as shown in this paper, is the mixture with 11mm NMAS (PA11) and it is used as 40 mm wearing courses. Material properties of PA11 based on European standard are summarized in Table 1 (14). The grain size distribution of PA11 is shown in Figure 1 and it also shows the upper and lower limit bounds.

There have been many applications to asphalt pavements using reinforcement materials such as steel grids, geotextile, and glass fibers. However, reinforcement of asphalt pavements with grids has attracted much attention and has triggered international initiatives such as the European Cost 348 REIPAS (15). Nowadays, a considerable variety of different reinforcement products and systems are available and still under development raising questions about appropriate applications. As shown in Figure 2(a), carbon FRP grids are composed of transverse carbon fibers and longitudinal glass fibers and the grids were coated by Styrene-Butadiene-Styrene (SBS) polymer modified binder and chipped by fine sands to increase the surface roughness. The theoretical cross-sections for both glass and carbon fibers are $50mm^2/m$. The mesh width; the distance between the neighboring fiber grids in longitudinal and transverse directions, is 20mm. The detail material properties of carbon FRP grids used in this study are shown in Figure 2(b).

EXPERIMENTAL TESTS AND RESULTS

Coaxial Shear Test

The Coaxial shear test (CAST), as shown in Figure 3, was designed at Empa, in the 1980s and has been continuously developed further and improved (16). The CAST determines the mechanical properties of ring-shaped asphalt specimens under dynamic load cycles and temperature changes. It is also able to perform modulus tests at wet condition. Inner and outer lateral surfaces of the specimens are sealed with epoxy resin and then glued to an internal steel core and an external steel ring respectively. Afterwards, the specimen with the steel ring is placed into the climatic testing chamber and mounted on a loading platform while the steel core is connected to the servo-hydraulic testing system. The outer diameter of CAST specimen is 150mm and the specimen height is 50mm. The detail specimen dimension can be found in Figure 3(b). The CAST set-up for specimen testing in water has been described in detail elsewhere (17). The repeatability of test results is within 2% to 3%.

Temperature in the climatic chamber can be changed in saw-tooth temperature cycles and controlled with a tolerance of ±0.2°C. The servo-hydraulic system provides axial sinusoidal load cycles in controlled stress and strain mode. In particular, for the wet test, sinusoidal loading cycles are selected to simulate the pressure-pumping effect of water in the asphalt mixture cavities. The displacement is measured on the upper surface of the steel core by means of an LVDT. Using the data acquisition software and the integrated finite element model, complex modulus $|E^*|$ and phase angle are calculated taking into account the glue properties and geometry of the test set-up. In this study, coaxial shear tests were conducted under the following testing program:

- Temperature(°C): 10, 15, 20, 25, 30
- Frequency (Hz): 0.125, 0.25, 0.5, 1, 2, 4, 8, 16
- Load amplitude (kN): 0.1, 0.32, 1

The modulus of test specimen was calculated using the following formula and the iterative coefficient function was derived by the finite element analysis (FEA) (18):

$$G^* = \frac{F_a}{\delta_a} A(G^*) \tag{1}$$

Where:

G^* = Complex modulus in shear,

F_a = Force amplitude along the steel core,

δ_a = Displacement amplitude along the steel core,

$A(G^*)$ = Coefficient function derived from FEA by recursive iteration

The method of time temperature superposition was used to construct master curves at the reference temperature (25°C) based on Witczak's sigmoidal function (19):

$$\log|E^*| = \delta + \frac{\alpha}{1 + e^{\beta - \gamma(\log f_r + \log a_T)}} \tag{2}$$

Where,

E^* = Complex modulus,

δ = Parameter describing the minimum value of G^*,

f_r = Frequency of loading at the reference temperature,

α = Parameter describing the span between max and min value of G^*,

β, γ = Parameter describing the shape of the sigmoidal function,

a_T = Shift factor, determined with Williams-Landel-Ferry (WLF) relationship

The shift factor (a_T) is determined by Eq.3: where, T = temperature; T_R = reference temperature; C_1 and C_2 are WLF constant coefficients.

$$\log(a_T) = \frac{-C_1 \times (T - T_R)}{C_2 + T - T_R} \tag{3}$$

The conversion equation to convert the measured shear stiffness $|G^*|$ to extensional complex modulus $|E^*|$ were employed. The theoretical approach using Poisson's ratio of 0.35 was assumed.

Due to its high porosity, porous asphalt ages much faster than conventional dense mixes. The mixes have been in short-term (STOA) and long-term oven aged (LTOA) conditions in accordance to the AASHTO Provisional Standards (20). Short term aging simulates the pre-compaction phase of the construction phase, and long term aging simulates aging that occurs over the service life of the pavement. In the first step, for STOA, laboratory-prepared loose mix asphalt was placed in a pan and spread to a thickness of 30mm - 40mm and condi-

tioned in a forced draft oven for 4 hour ± 5 minutes at the mixture compaction temperature. Thereafter, for LTOA, the loose mix from STOA was used to prepare the specimens which were then aged in a forced draft oven at 85±3°C for 120±0.5 hours.

The CAST results for porous asphalt in Figure 4(a) show an increase in the modulus due to aging especially at lower frequencies. The CAST results from unaged specimens show a wide range of phase angle than those of aged specimens. Properties of PA can be influenced by water exposure as shown in the example in Figure 4(c) and Figure 4(d). In order to determine the material sensitivity in the presence of water, CAST fatigue tests were performed in a dry state and under water. The tested temperatures were -10, -5, 0, 5, 10, 15, 20, 25, 30 °C and the frequency range was 0.25, 0.5, 1, 2, 4, 8, 16 Hz. In order to simulate field conditions, the mechanical properties of specimens under combination of repeated loading, water immersion, and temperature cycles were applied. For example, it can be seen that the wet PA specimen is already displaying a reduction in complex modulus after the third cycle of loading in comparison to the dry specimen (Figure 4(d)). All test results are average of two replicates.

Accelerated Pavement Fatigue Test

Test Equipment and Specimen Preparation

A model mobile load simulator (MMLS) was used to apply the accelerated fatigue traffic loadings on fiber-reinforced porous asphalt composite specimens as shown in Figure 5(a). The accelerated pavement fatigue tests were conducted at 25±1.0°C. Figure 5(b) and Figure 5(c) shows the dimension of MMLS and its detail specifications. The width of MMLS is 600mm and the maximum number of cycles is 0.5 million.

The selected specimen dimension was 1,800mm length, 870mm width, and 60mm thickness. The specimen size was chosen to be larger than 1,200mm MMLS loading length and 600mm MMLS width. Four two-layered specimens were produced using PA11 for testing with the MMLS. The specimens were compacted with a vibration roller compactor. As shown in Table 2, the thickness of bottom layer was 20mm with dense asphalt concrete (AC8) as a binder course and the thickness of top layer was 40mm with porous asphalt based on the recommendation of wearing course by Swiss standard. K1 and K2 composite systems were tested at dry condition but the reinforcement was not placed into K1 specimen. K3 and K4 composite systems were tested at wet condition to investigate the water sensitivity.

The procedure for preparing fatigue test specimens are in four steps:

1) Placing the hot-mix asphalt into the roller compactor and compacting the bottom AC8 layer (Figure 6(a))
2) After cooling of the bottom AC8 layer, 5mm top surface is milled off and then polymer-modified emulsion including 60% asphalt binder is applied on the top surface as a bonding material (Figure 6(b))
3) Applying the flame to the emulsion and the surface of carbon FRP grids to have better bond conditions after drying the polymer-modified emulsion (Figure 6(c))
4) Compacting the top porous asphalt (PA11) layer after placing carbon FRP grids (Figure 6(d))

The bottom asphalt layer of specimen was produced with an additional thickness of 5mm (total thickness 25mm). Before applying the reinforcement grid, these additional 5mm were milled off with a hand miller, resulting in a final thickness of 20mm. In order to simulate the compliance of the subbase, the specimens were supported by a cellular rubber pad with 12mm thickness and with 0.19MPa elastic modulus as shown in Figure 6(e). Also, K3 and K4 specimens were placed in a water bath with 20mm water level below the top surface of specimen.

In order to measure the strain responses during MMLS testing, strain gauges (in German, Dehnungsmessstreifen DMS) were installed on the bottom of porous asphalt layer, 40mm from the top surface, as shown in Figure 7. One DMS was arranged longitudinally (DMS1) and two in the transverse direction (DMS2 on the bottom side and DMS3 on the top side). These DMS strips with 120mm length are in a plastic bag and their elastic modulus, 2.75GPa, is close to that of normal asphalt concrete at room temperature.

FATIGUE TEST RESULTS AND DISCUSSIONS

Strain Results

The strain responses have been measured during the entire MMLS testing and the strain gauges measured the data for 30 seconds every hour. Each channel stored 100 measurements per second. Figure 8 shows the measured strains of reference specimen (K1) in the beginning of testing. Each peak value of strain curves corresponds to the individual tire loading of MMLS. Table 3 shows the average strain amplitudes, the differences between neighboring local maximum and minimum values such as point A and point B in Figure 8. The amplitude of transverse strains was larger than amplitude of longitudinal strains. The transverse strains decreased by 10% at dry and by 15% at wet condition when the reinforcement is applied. Additionally, the ratio between transverse (DMS2) and longitudinal (DMS1) strains decreased for fiber-reinforced specimens by 9% at dry condition and by 25% at wet condition.

Transverse Surface Profiles

During MMLS testing, the transverse profiles of surface deflection were measured from the cross section in the middle of the specimen by the surface profilometer. Figure 9 shows the transverse surface profiles for all tested specimens at different fatigue loading cycles. Due to the faster specimen failures, specimens tested at wet conditions (Figure 9(c) and Figure 9(d)) have fewer profile curves compared with specimens tested at dry condition. The maximum deflection at dry condition under the wheel path was 7.648mm without reinforcement and 5.868mm with reinforcement at 370,000 cycles (Figure 9(a) and Figure (b)). The deflection reduction of reinforced specimen was 23% at dry condition. Also, the maximum deflection at wet condition was 4.777mm without reinforcement and 2.476mm with reinforcement at 150,000 cycles (Figure 9(c) and Figure 9(d)). The surface deflection of reinforced specimen was significantly reduced with 48% reduction ratio. As summarized in Figure 10, the fiber reinforcement significantly affected the surface deflections at both dry and wet conditions. However, the deflections at wet condition were less than those at dry condition. The lower deflections at wet condition came from localized surface failures on the wheel path, which was due to less adhesion by moisture damage.

Specimen Failures

Table 4 shows the number of loading cycles for all test specimens until the full-depth longitudinal fatigue cracks occurred. At dry condition, the unreinforced specimen had the full-depth fatigue cracks between 310,000 and 320,000 cycles. On the other hand, the reinforced specimen had the full-depth fatigue cracks between 380,000 and 390,000 cycles. Also, at wet condition, the unreinforced and reinforced specimens had the full-depth fatigue cracks at around 220,000 and around 280,000 cycles respectively. Based on the MMLS fatigue test results, the fiber reinforcement improved the fatigue crack resistance both at dry and wet conditions. Figure 11 compared the specimen failure results for all four specimens at the end of MMLS tests. Figure 11(a) shows the top and bottom side of unreinforced specimen at dry condition. Figure 11(b) shows both top and bottom sides of reinforced specimen tested at dry condition. The unreinforced specimen had many fatigue cracks at bottom side while the reinforced specimen had much less fatigue cracks. Figure 11(c) and Figure 11(d) show the top sides of unreinforced and reinforced specimens tested at wet condition. The unreinforced specimen tested at wet condition showed significant stripping with wider and deep failures on the surface. The reinforcement materials improved the fatigue performance and the durability of porous asphalt.

SUMMARY AND CONCLUSIONS

This paper introduced the application of carbon FRP grids to improve the fatigue resistance of porous asphalt. The aging and moisture sensitivity of porous asphalt were investigated by the Swiss CAST test. The MMLS was successfully used as an accelerated pavement testing equipment to apply dynamic fatigue traffic loadings on the surface of specimens. The fatigue behaviour for both reinforced and unreinforced specimens was observed and measured by installed strain gauges and the surface profilometer. The fatigue tests were performed at both dry and wet condition to compare the water sensitivity and to investigate the performance improvement by reinforcement materials. However, further analyses on quantifying the benefit of grid system are still needed and should be incorporated in the pavement design method. Based upon the findings of this study, the following conclusions are drawn:

- The use of interlaid carbon FRP grids to porous asphalt led to the improvement of fatigue resistance of porous asphalt when MMLS fatigue loadings were applied.
- The CAST results showed the stiffness hardening of porous asphalt by aging and it was significant at lower loading frequencies. The aged specimens showed higher stiffness with the minimum of 25% and the maximum of 55%. Also, CAST results tested at wet condition proved that the water sensitivity of porous asphalt is an important factor due to significant reduction in stiffness.
- Based on the strain and deflection measurements during the MMLS fatigue loading, the transverse strain of porous asphalt specimen decreased by fiber reinforcement by 10% at dry condition and by 15% at wet condition. The surface deflection reduction by reinforcement materials was 23% at dry condition and 48% at wet condition.
- Carbon FRP-reinforced specimens had longer fatigue life by 23% at dry condition and by 27% at wet condition based on the number of loading cycles when the full-depth fatigue cracks occurred. Also, failed porous asphalt specimens without reinforcement materials showed more fatigue cracks on the bottom side and more stripping on the top loading surface.

REFERENCES

1. Takahashi, S. and M.N. Partl. *Improvemenet of Mix Design for Porous Asphalt*. Empa, Swiss Federal Laboratories for Materials Testing and Research, Research Report Number 840221, Dübendorf, Switzerland, 1999.

2. Poulikakos, L.D., S. Takahashi, and M.N. Partl. *Evaluation of Improved Porous Asphalt by Various Test Methods*. Empa, Swiss Federal Laboratories for Materials Testing and Research, Research Report Number 860076, Dübendorf, Switzerland, 2006.

3. Poulikakos, L.D., R. Gubler, M.N. Partl, M. Pittet, A. Junod, and E. Simond. Current State of Porous Asphalt in Switzerland. *Proceedings of the Tenth International Conference on Asphalt Pavements*. Quebec, Canada, 2006.

4. Barrett, M.E. and C.B. Shaw. Benefits of Porous Asphalt Overlay on Storm Water Quality. *Transportation Research Record*, Vol. 2025, pp.127-134, 2008.

5. Tan, S.A., T.F. Fwa, and K.C. Chai. Drainage Considerations for Porous Asphalt Surface Course Design. *Transportation Research Record*, Vol. 1868, pp.142-149, 2007.

6. Moore, L.M., R.G. Hicks, and D.F. Rogge. Design, Construction, and Maintenance Guidelines for Porous Asphalt Pavements. *Transportation Research Record*, Vol. 1778, pp.91-99, 2007.

7. Hoban, T.W.S., F. Liversedge, and R. Searby. Recent Developments in Pervious Macadam Surfaces. *Proceedings of the Third Eurobitumen Symposium*, Hague, Netherlands, pp.635-640, 1985.

8. Nicholls, J.C. *Review of UK Porous Asphalt Trials*. Transport Research Laboratory, TRL Report 264, Crowthorne, England, 1996.

9. Potter, J.G. and A.R. Halliday. *The Contribution of Pervious Macadam Surfacing to the Structural Performance of Roads*. Transportation Research Laboratory, TRL Report 1022, 1981.

10. Swiss Standards. *Bituminous Mixtures - Material Specifications - Part 7:Porous Asphalt*. Association of Swiss Road and Traffic Engineers (VSS), SN 640431-7a, 2008.

11. Gerardu, J.J.A., F.A. Hansen, C. Jonker, and J.J. van der Plas. The use of Porous Asphalt Wearing Courses in the Netherlands. *Proceedings of the Third Eurobitumen Symposium*, Hague, Netherlands, pp.676-685, 1985.

12. Japan Highway Publich Corporation. *Design and Execution Manual for Porous Asphalt; Haisuisei-hosou Sekkei Sekou Manual*. Tokyo, Japan, 1994.

13. European Standards. *Bituminous Mixtures - Material Specifications – Part 7: Porous Asphalt.* European Committee for Standardization (CEN), EN 13108-7, 2008.

14. European Standards. *Bituminous Mixtures - Test Methods for Hot Mix Aspahlt.* European Committee for Standardization (CEN), EN 12697, 2004.

15. Rathmayer, H. *Reinforcement of Pavements with Steel Meshes and Geosynthetics*. European Cooperation in the Field of Scientific and Technical Research (COST), COST 348 REIPAS, 2006.

16. Gubler, R., L.G. Baida, and M.N. Partl. A New Method to Determine the Influence of Water on Mechanical Properties of Asphalt Concrete. *International Journal of Road Materials and Pavement Design; Special Issue of the First EATA Conference*, pp.259-279, 2004.

17. Gubler, R., M.N. Partl, F. Canestrari, and A. Grilli. Influnce of Water and Temperature on Mechanical Properties of Selected Asphalt Pavements. *RILEM Materials and Stuctures*, Vol.38, pp.523-532, 2005.

18. Sokolov, K., R. Gubler, and M.N. Partl. Extended Numerical Modeling and Application of the Coaxial Shear Test for Asphalt Pavements. *RILEM Materials and Stuctures*, Vol.38, pp.515-522, 2005.

19. Fonseca, O.A. and M.W. Witczak. A Prediction Methodology for the Dynamic Modulus of In Place Aged Asphalt Mixture. *Journal of the Association of Asphalt Paving Technologist*, Vol. 65, pp.532-565, 1996.

20. AASHTO Provisional Standards. *Standard Practice for Short Term and Long Term Aging of Hot Mix Asphalt (HMA)*, American Association of State Highway and Transportation Officials (AASHTO), pp.2-96, 2001.

List of Tables

List of Figures

TABLE 1 Asphalt binder and mixture properties

	Properties	PA 11
Marshall Specimen	Percentage of Binder (Mass %)	4.90
	Density (kg/m^3)	2466
	Area Density, SSD (kg/m^3)	1967
	Percentage of Air Void (Vol.%)	20.2
	Voids Filled with Asphalt, VFA (Vol.%)	31.6
Marshall Properties	Marshall Stability (kN)	6.0
	Marshall Flow (mm)	3.8

TABLE 2 Asphalt concrete specimens, system characteristics

Specimen	Test condition	Thickness t1 bottom AC layer [mm]	Thickness t2 top PA layer [mm]	Carbon FRP grid position	
				From top [mm]	Reinforcement
K1	Dry	20	40	0	No Reinforcement
K2	Dry	20	40	40	Reinforcement
K3	Wet	20	40	0	No Reinforcement
K4	Wet	20	40	40	Reinforcement

TABLE 3 Measured average strain amplitudes

Specimen	Test condition	Average amplitude of strain (%)			DMS2/DMS1 (Trans./Long.)
		DMS1	DMS2	DMS3	
K1	No reinforcement	0.0224	0.0298	- 0.00490	1.33
K2	Reinforcement	0.0222	0.0268	- 0.00710	1.21
K3	No reinforcement	0.0192	0.0260	- 0.00509	1.35
K4	Reinforcement	0.0218	0.0221	- 0.00585	1.01

TABLE 4 Number of loading cycles at full-depth longitudinal fatigue cracks

Specimen	Test condition	Reinforcement	Number of cycles until full-depth longitudinal cracks	Number of cycles at test end
K1	Dry	No	310,000 – 320,000	500,000
K2	Dry	Yes	380,000 – 390,000	500,000
K3	Wet	No	220,000 – 230,000	320,000
K4	Wet	Yes	280,000 – 290,000	500,000

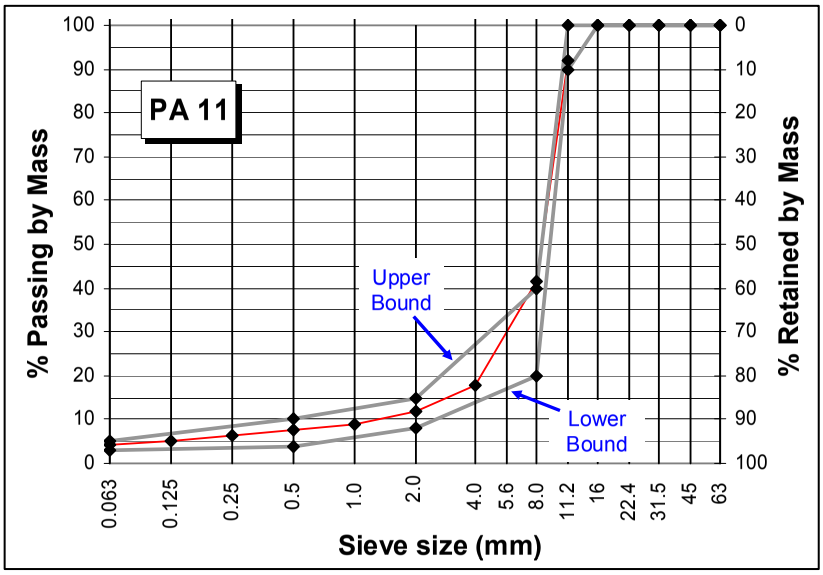

FIGURE 1 Aggregate gradation curve of PA11.

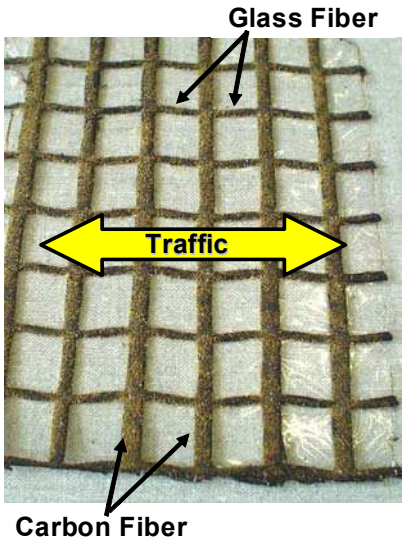

Carbon FRP Grid			
Fiber Type	Tensile Modulus (GPa)	Ultimate Strain (mm/mm)	Ultimate Force (kN/m)
Carbon Fiber (Transverse)	240	0.015	200
Glass Fiber (Longitudinal)	73	0.03 – 0.045	120

(a) **(b)**

FIGURE 2 Details of Carbon FRP grid: (a) carbon FRP grid; (b) material properties of carbon FRP grid.

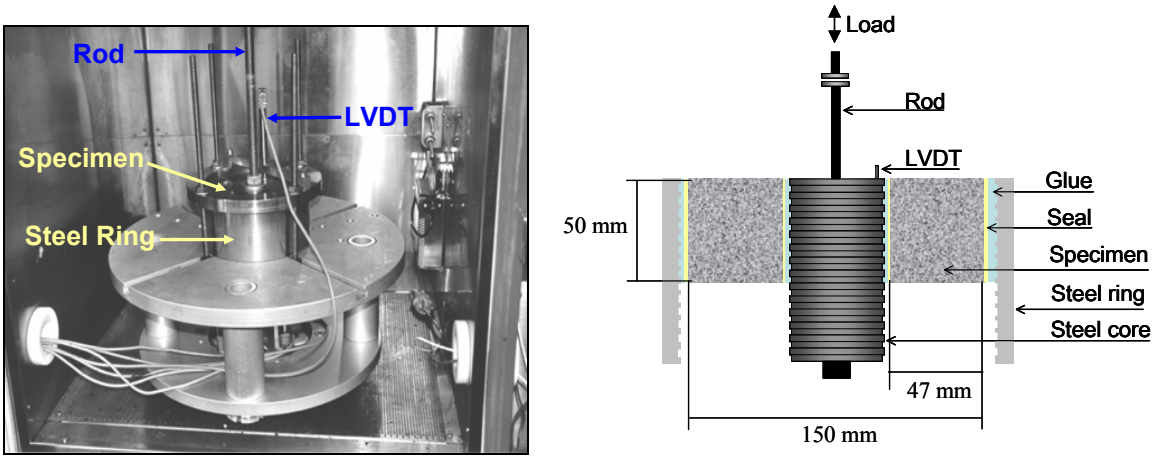

(a) (b)

FIGURE 3 Details of coaxial shear test: (a) test set-up; (b) test principle and dimension.

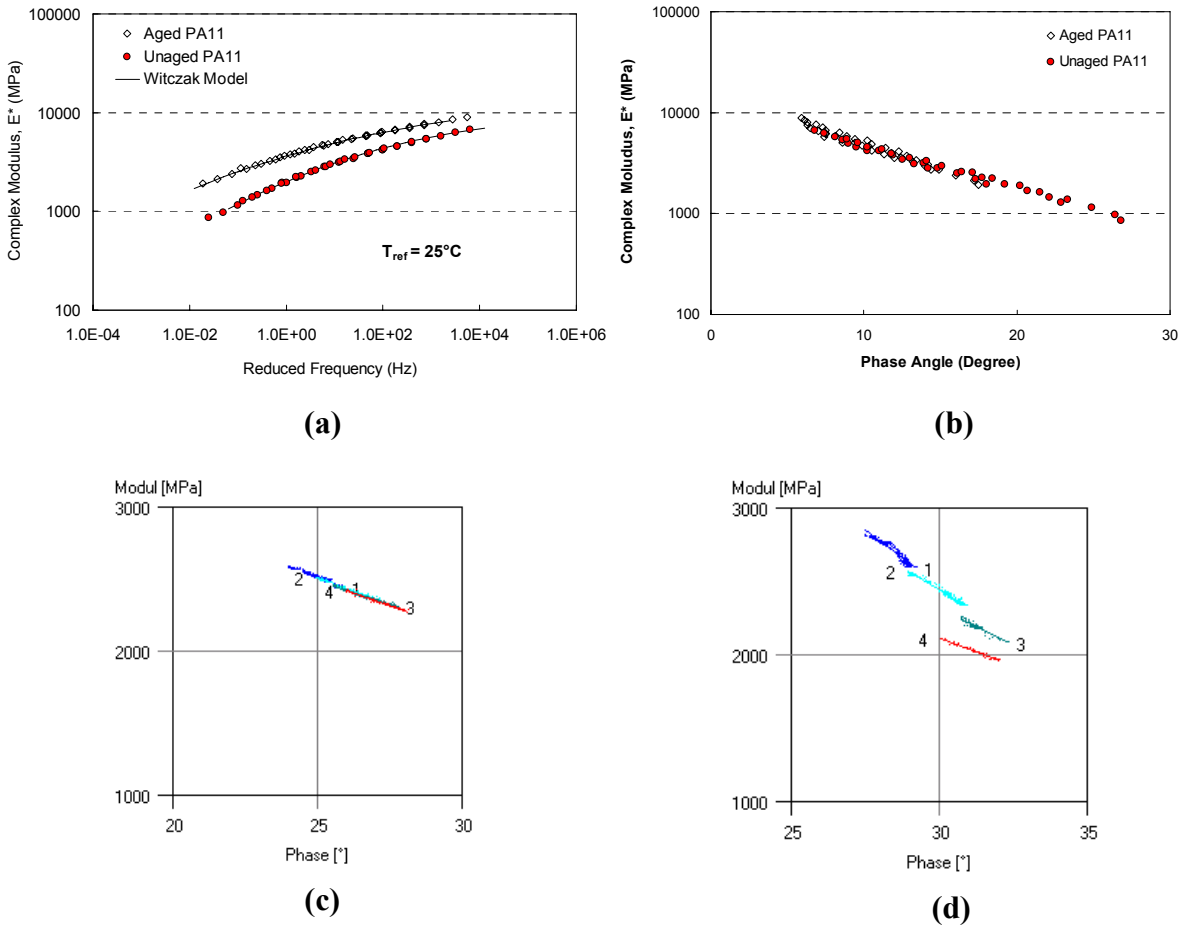

FIGURE 4 CAST test results: (a) master curves for aged and unaged PAs; (b) black diagrams for aged and unaged PAs; (c) black diagram at dry condition; and (d) black diagram at wet condition.

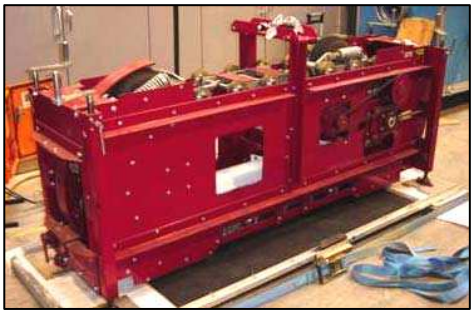

(a)

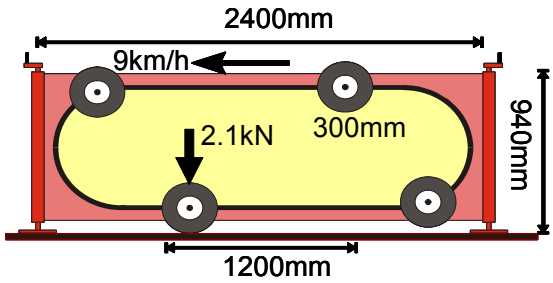

(b)

Weight (kg)	800
Evaluated track length (mm)	1,000
Tire diameter (mm)	300
Tire width (mm)	80
Tire pressure (MPa)	0.6
Load per tire (kN)	2.1
Speed (km/h)	9
Number of cycles per hour	7,200
Maximum number of cycles	0.5 million

(c)

FIGURE 5 Details of model mobile load simulator (MMLS): (a) MMLS placed on the top surface of specimen; (b) dimension of MMLS; and (c) specifications of MMLS.

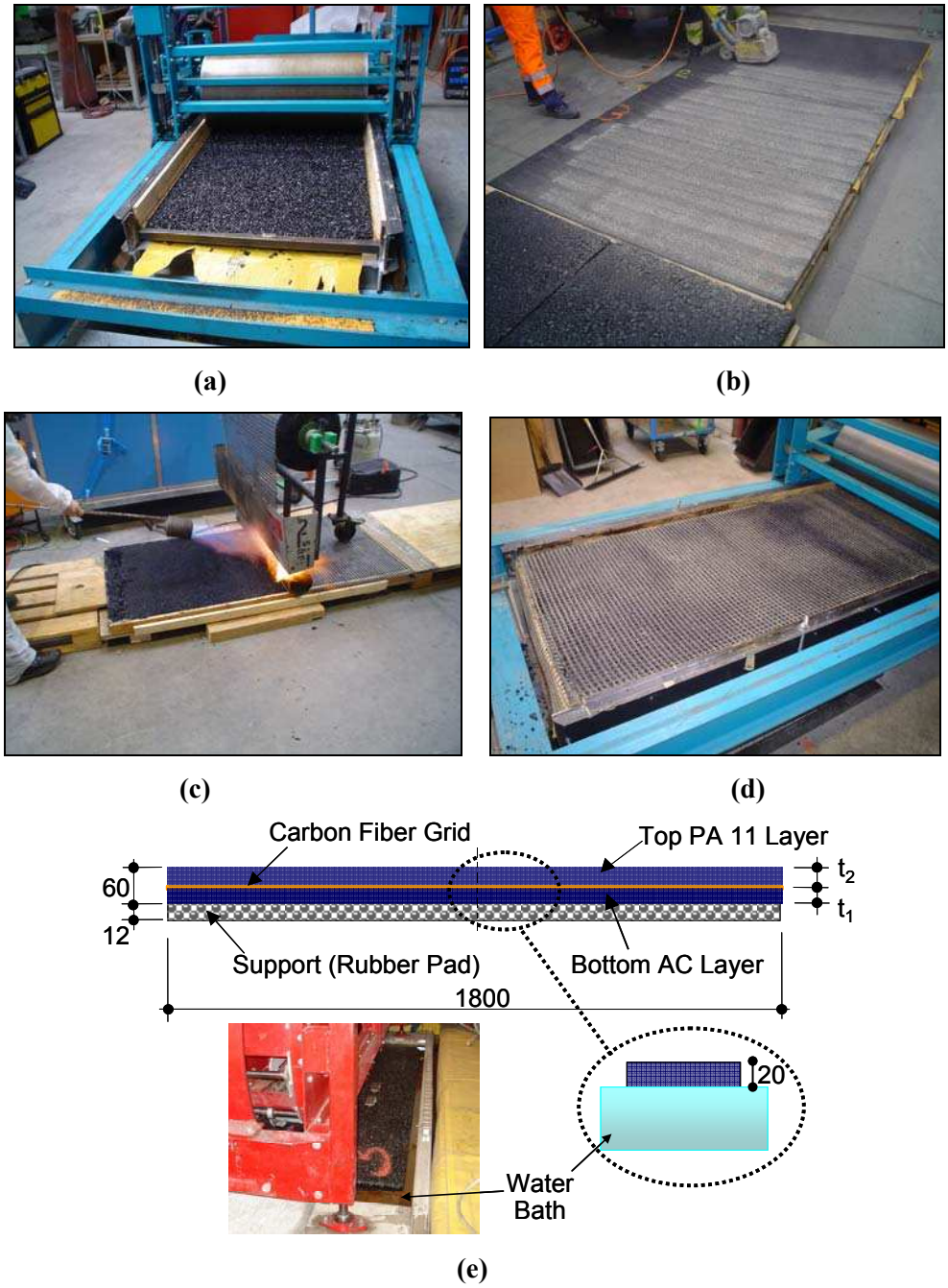

FIGURE 6 Specimen preparation: (a) compaction of bottom AC layer; (b) milling off the compacted AC top surface; (c) placing carbon FRP grids and bonding by flame; (d) before applying upper porous asphalt layer; and (e) specimen in a water bath.

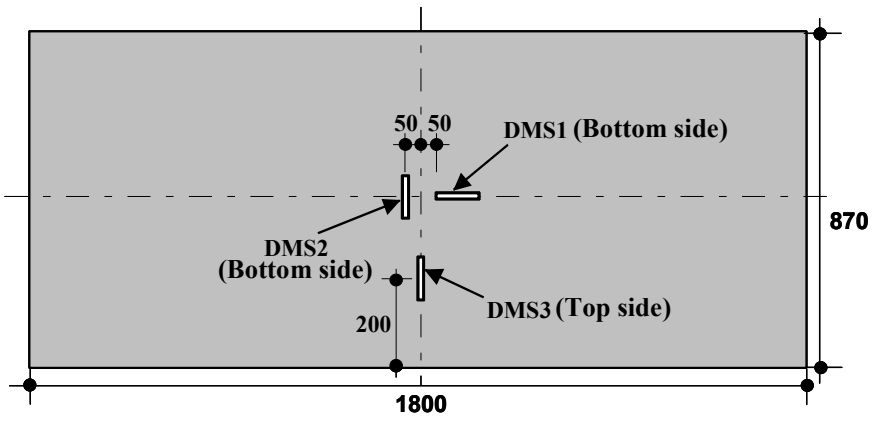

FIGURE 7 Installed strain gauge locations (unit: mm).

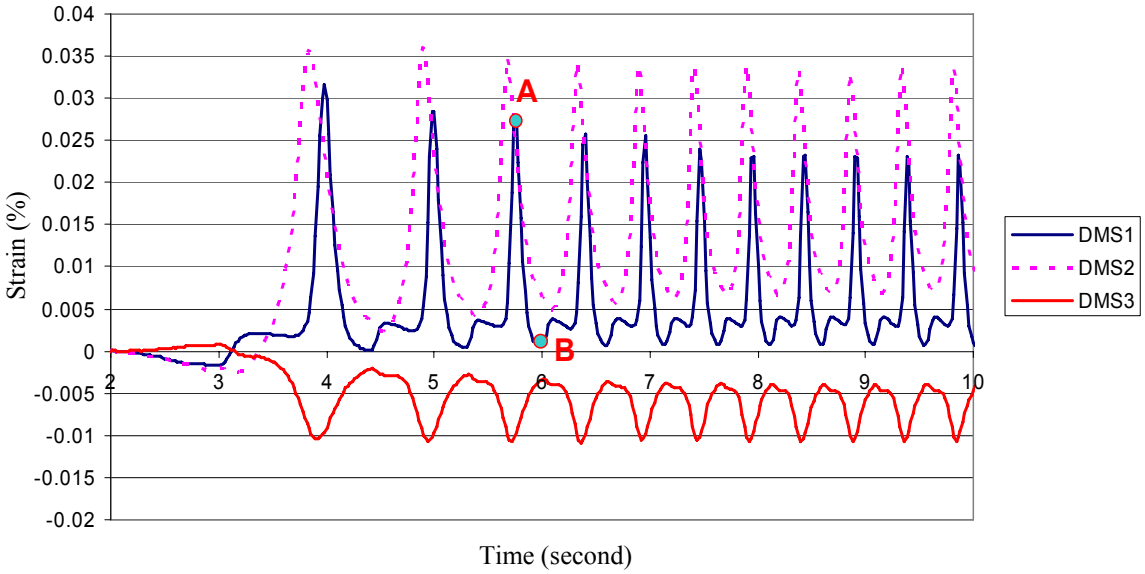

FIGURE 8 Initial strain measurements (K1).

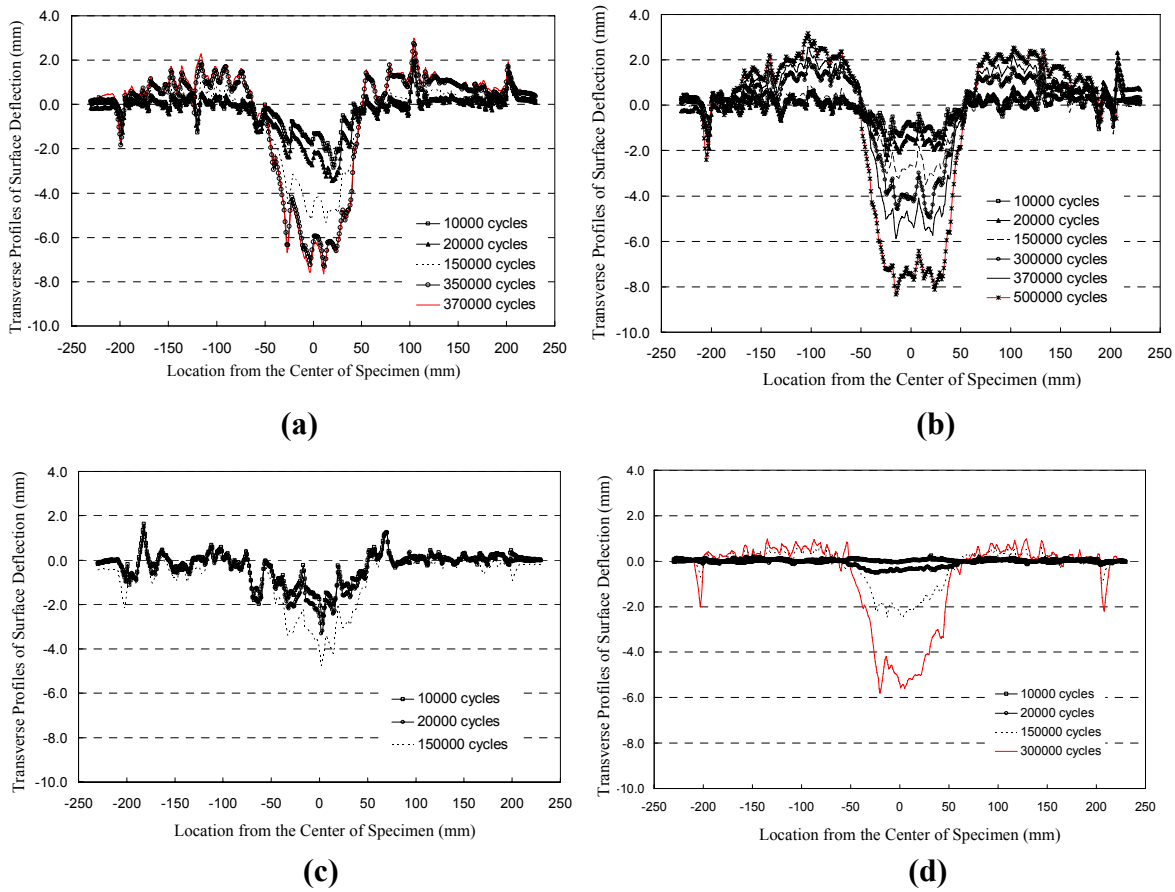

FIGURE 9 Transverse profiles of surface deflection: (a) unreinforced at dry (K1); (b) reinforced at dry (K2); (c) unreinforced at wet (K3); and (d) reinforced at wet (K4).

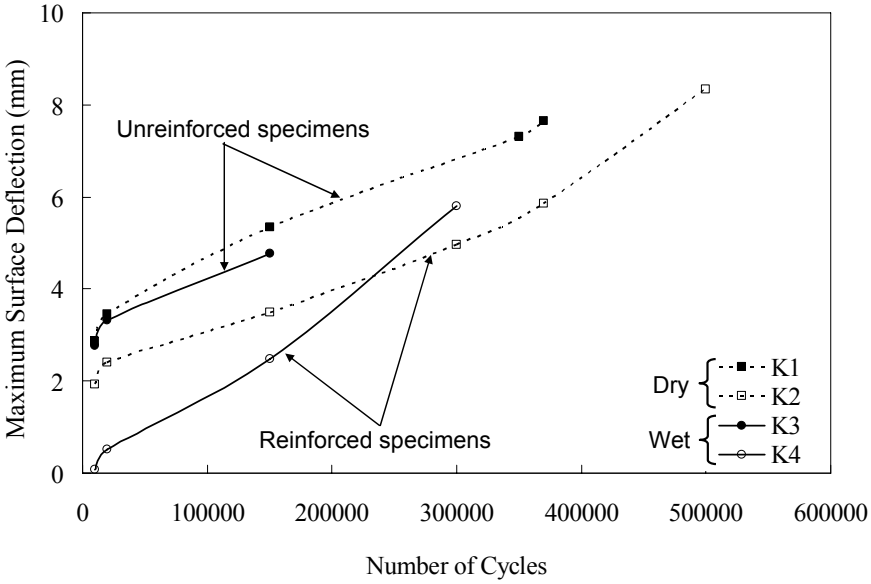

FIGURE 10 Comparison of maximum surface deflection.

(a)

(b)

(c) **(d)**

FIGURE 11 Specimen failures after MMLS tests: (a) K1 top (left) and bottom side (right); (b) K2 top (left) and bottom side(right); (c) K3 top side; and (d) K4 top side.